

# Proca in the sky

Lavinia Heisenberg\*, Hector Villarrubia-Rojo†

*Institute for Theoretical Physics, ETH Zürich, Wolfgang-Pauli-Strasse 27, 8093, Zürich, Switzerland*

(Dated: February 9, 2022)

The standard model of cosmology, the  $\Lambda$ CDM model, describes the evolution of the Universe since the Big Bang with just a few parameters, six in its basic form. Despite being the simplest model, direct late-time measurements of the Hubble constant compared with the early-universe measurements result in the so-called  $H_0$  tension. It is claimed that a late time resolution is predestined to fail when different cosmological probes are combined. In this work, we shake the ground of this belief with a very simple model. We show how, in the context of cubic vector Galileon models, the Hubble tension can naturally be relieved using a combination of CMB, BAO and SNe observations *without* using any prior on  $H_0$ . The tension can be reduced even further by including the local measurement of the Hubble constant.

## Contents

<b>I. Introduction</b>	<b>1</b>
<b>II. A simple Generalized Proca model</b>	<b>2</b>
<b>III. The background evolution</b>	<b>3</b>
A. Dark energy model	4
B. Physical effects	4
<b>IV. Perturbations</b>	<b>6</b>
A. Dark energy model	7
B. Physical effects	8
<b>V. Observations</b>	<b>10</b>
A. Observational constraints	11
B. $H_0$ tension	11
C. Complementary observations: $\sigma_8$ and ISW effect	13
<b>VI. Summary and conclusions</b>	<b>15</b>
<b>Acknowledgments</b>	<b>16</b>
<b>A. General perturbations</b>	<b>16</b>
<b>B. Super- and sub-Hubble analysis</b>	<b>17</b>
1. Super-Hubble limit	17
2. Sub-Hubble limit	18
<b>References</b>	<b>18</b>

## I. INTRODUCTION

The standard model of cosmology rests on two fundamental pillars, the cosmological principle and General Relativity. The former states that the observable properties of the Universe are isotropic and homogeneous, which on the

---

\* lavinia.heisenberg@phys.ethz.ch

† herojo@phys.ethz.ch

other hand enables to find exact solutions to Einstein's field equations. In the standard formulation of General Relativity (see [1, 2] for alternative formulations) the fundamental object is the symmetric  $4 \times 4$  metric tensor,  $g_{\mu\nu}$ . The cosmological principle greatly simplifies the metric to be of the Friedmann-Lemaître-Robertson-Walker form, where the dynamics given by Einstein's field equations are solely captured by the scale factor. Matter fields are represented by the homogenous and isotropic energy-momentum tensor in form of pressure and energy density. The governing equations can be brought into a single equation for the Hubble parameter  $\mathcal{H} = \dot{a}/a$  as a function of dimensionless density parameters

$$\mathcal{H}^2 = a^2 H_0^2 (\Omega_r a^{-4} + \Omega_m a^{-3} + \Omega_K a^{-2} + \Omega_\Lambda) , \quad (1)$$

with the density parameters of radiation  $\Omega_r$ , non-relativistic matter  $\Omega_m$ , curvature  $\Omega_K$  and cosmological constant  $\Omega_\Lambda$ , and the Hubble constant  $H_0$ . Even though this simple  $\Lambda$ CDM model is in good agreement with cosmological observations, the Hubble tension has created a growing concern. The distance scale measurement of the Hubble constant based on Cepheids from the SH0ES collaboration gave a value  $H_0 = 74.03 \pm 1.42$  [3], which is more than  $4\sigma$  away from the value inferred from Planck  $H_0 = 67.44 \pm 0.58$  [4]. This discrepancy may be due to systematic errors, but it could also signal deviations from the  $\Lambda$ CDM model. In this work, we will assume the latter. We will consider an extension of the standard model in the presence of an additional vector field, playing the role of dark energy. It is claimed that if the Hubble tension is resolved through modifications in the late time universe, this will be very difficult to reconcile with early universe measurements like BAO. Here, we show with a very simple model of a vector Galileon how this belief is easily circumvented.

Mostly studied extensions of the  $\Lambda$ CDM model are based on an additional scalar field. In the cosmological context, theories of the scalar Galileon and Horndeski [5–7] have received quite some attention. Simple scalar models like Quintessence generically fail to address the Hubble tension [8]. Cubic Horndeski and Galileon type of scalar theories typically fail to reconcile different cosmological measurement including the ISW-galaxy density cross-correlations [9]. On the other hand, as it was shown in [10] for the first time, simple vector models can readily alleviate the Hubble tension due to a phantom-like behaviour of the background. The background analysis was further extended to linear perturbations in [11]. Here, we present the results of our own implementation into a Boltzmann code based on CLASS [12], using also MontePython [13, 14] to constrain the cosmological parameters and GetDist [15] to analyze the posteriors and plot the results. We will consider a specific model of the cubic Generalized Proca (GP) theory. It represents a simple but rich subclass of Generalized Proca interactions [16–18].

This paper is organized as follows. In Section II we present the subclass of Generalized Proca models that we focus on. Section III analyzes the cosmological behaviour of the GP model at the background level. Section IV extends the analysis to include perturbations. In Section V we constrain the free parameters of the model, performing a detailed comparison with observational data, and address the Hubble tension. Finally, Section VI gathers the main results and discusses some prospects for future work.

## II. A SIMPLE GENERALIZED PROCA MODEL

Galilean interactions for a spin-1 field can only be constructed for the massive case. These are the Generalized Proca theories [2, 16–18]. They constitute the most general Lagrangians for a massive vector field with derivative self-interactions, which nevertheless give rise to second order equations of motion and propagate 3 physical modes. From the six possible Lagrangians we will consider only a simple subclass, which also automatically satisfies the bounds on the gravitational waves speed. The generalized Proca theories have opened up a promising avenue for phenomenological applications in cosmology and black hole physics [19–23]. In this work, we are interested in its cosmological implications, specially in the context of the Hubble tension. The action for the model that we consider is

$$S = \int d^4x \sqrt{-g} \{ G_4 R + \alpha F + G_2(X) + G_3(X) \nabla^\mu A_\mu \} , \quad (2)$$

with the short-cut notations introduced

$$F \equiv -\frac{1}{4} F^{\mu\nu} F_{\mu\nu} , \quad X \equiv -\frac{1}{2} A^\mu A_\mu , \quad G_4 \equiv \frac{1}{16\pi G} . \quad (3)$$

The energy-momentum tensor, defined as

$$T_{\mu\nu} \equiv -\frac{2}{\sqrt{-g}} \frac{\delta S_{\text{Proca}}}{\delta g^{\mu\nu}} , \quad (4)$$

is given by the following

$$T_{\mu\nu} = \alpha \left( F_\mu{}^\rho F_{\nu\rho} + F g_{\mu\nu} \right) + g_{\mu\nu} G_2 + A_\mu A_\nu G_{2,X} \\ + G_{3,X} \left( A_\mu A_\nu \nabla_\rho A^\rho - A^\rho (A_\mu \nabla_\nu A_\rho + A_\nu \nabla_\mu A_\rho) + g_{\mu\nu} A^\rho A^\sigma \nabla_\rho A_\sigma \right). \quad (5)$$

The equations of motion of the vector field can be obtained as

$$\mathcal{E}_\mu \equiv \frac{\delta S_{\text{Proca}}}{\delta A^\mu} = 0, \quad (6)$$

and we have

$$\mathcal{E}_\mu = \alpha \nabla_\nu F^\nu{}_\mu - A_\mu G_{2,X} - G_{3,X} \left( A_\mu \nabla_\nu A^\nu - A_\nu \nabla_\mu A^\nu \right). \quad (7)$$

In the following section we will adapt the theory to the symmetries of the cosmological background, specify further the model and discuss the background observables.

### III. THE BACKGROUND EVOLUTION

For any given model its confrontation with cosmological observations is a crucial ingredient in testing the underlying theory. A natural starting point is the study of the background evolution. Using the distance-redshift relation from Supernovae, BAO measurements and the full CMB data from *Planck*, the parameters of the model can successfully be constrained. We will now particularize the results of the covariant equations in the previous section to a FLRW metric

$$ds^2 = a^2(\tau)(-d\tau^2 + d\mathbf{x}^2), \quad (8)$$

and a field configuration for the vector field

$$A^0 \equiv \frac{1}{a}\phi(\tau), \quad A^i = 0. \quad (9)$$

The equation of motion of the vector field (7) simplifies to

$$\mathcal{E}_0 = \phi(aG_{2,X} + 3\phi\mathcal{H}G_{3,X}) = 0, \quad (10a)$$

$$\mathcal{E}_i = 0. \quad (10b)$$

The energy-momentum tensor (5), on the other hand, particularizes into

$$T^0_0 = G_2 - \phi^2 G_{2,X} - 3a^{-1}\mathcal{H}\phi^3 G_{3,X}, \quad (11a)$$

$$T^0_i = 0, \quad (11b)$$

$$T^i_j = \delta^i_j (G_2 - a^{-1}\phi^2 \dot{\phi} G_{3,X}), \quad (11c)$$

where  $\dot{\phantom{x}} \equiv d/d\tau$ . The usual fluid variables for the Proca field are

$$\rho_A = -G_2, \quad (12a)$$

$$P_A = G_2 + \frac{1}{3\mathcal{H}}\dot{G}_2, \quad (12b)$$

$$w_A = \frac{P_A}{\rho_A} = -1 - \frac{\dot{G}_2}{3\mathcal{H}G_2}. \quad (12c)$$

Deriving the constraint (10a) with respect to  $\tau$ , we get (for  $\phi \neq 0$ )

$$aG_{2,XX} = -3\phi\mathcal{H}G_{3,XX} - 3\phi^{-1}\mathcal{H}G_{3,X} - 3\dot{\phi}^{-1}(\dot{\mathcal{H}} - \mathcal{H}^2)G_{3,X}. \quad (13)$$

The Einstein equations yield the usual Friedmann equations plus the contribution from our dark energy fluid

$$\mathcal{H}^2 = \frac{8\pi G a^2}{3}\rho + \frac{8\pi G a^2}{3}P_A, \quad (14)$$

$$\dot{\mathcal{H}} - \mathcal{H}^2 = -4\pi G a^2(\rho + P) - 4\pi G a^2(\rho_A + P_A). \quad (15)$$

where  $\rho$  and  $P$  stand for the density and pressure of all the components except the Proca field.

### A. Dark energy model

Following the studies in [20, 21] we will consider a promising dark energy model, where the general functions are chosen to be polynomials

$$G_2(X) = b_2 X^{p_2} , \quad G_3(X) = b_3 X^{p_3} , \quad (16)$$

which yield from the constraint equation (10a)

$$\phi = \phi_0 \left( \frac{\mathcal{H}}{aH_0} \right)^{-1/p} , \quad (17)$$

where

$$p \equiv 1 - 2(p_2 - p_3) , \quad \phi_0 = \left( -\frac{2^{p_3} b_2 p_2}{3H_0 2^{p_2} b_3 p_3} \right)^{1/p} . \quad (18)$$

With the previous relations, the evolution of the density follows

$$\dot{\rho}_A = -\frac{2s}{\mathcal{H}} \left( \dot{\mathcal{H}} - \mathcal{H}^2 \right) \rho_A , \quad s \equiv \frac{p_2}{p} . \quad (19)$$

Using the Friedmann equations, it can also be rewritten as

$$\dot{\rho}_A = \frac{3\mathcal{H}(\rho + P)s\rho_A}{\rho + (1+s)\rho_A} , \quad (20)$$

where the equation of state in this case is

$$w_A = -1 - \frac{(1+w)s}{1 + (1+s)\rho_A/\rho} . \quad (21)$$

Finally, writing  $\rho_{\text{tot}} = \rho + \rho_A$ , we can reduce the differential equation to an algebraic one

$$-\frac{1}{s\rho_A} \frac{d\rho_A}{d \log a} = \frac{1}{\rho_{\text{tot}}} \frac{d\rho_{\text{tot}}}{d \log a} \quad \rightarrow \quad \rho_A \propto \rho_{\text{tot}}^{-s} = (\rho + \rho_A)^{-s} . \quad (22)$$

For later reference, we introduce the following short-hand notation

$$\mathcal{R} \equiv \frac{\rho_A}{\rho_{\text{tot}}} , \quad \tilde{\mathcal{R}} \equiv 1 - \mathcal{R} = \frac{\rho}{\rho_{\text{tot}}} , \quad \mathcal{X} \equiv -\frac{1+w_A}{s} = \frac{(1+w)\tilde{\mathcal{R}}}{1+s\mathcal{R}} . \quad (23)$$

Rewriting (19) in terms of these variables we have

$$\dot{\mathcal{R}} = \frac{3\mathcal{H}(s+1)(1+w)}{1+s\mathcal{R}} \mathcal{R}(1-\mathcal{R}) . \quad (24)$$

From this last expression we can see that, at late times, the Proca field evolves toward the de Sitter attractor  $\mathcal{R} \rightarrow 1$  and  $w_A \rightarrow -1$ .

### B. Physical effects

The concrete dark energy model that we have considered in (16) contains in principle four free parameters  $(b_2, b_3, p_2, p_3)$ . However, only two combinations of these parameters produce effects on the background. Assuming a flat universe, the value of the dark energy density today is fixed, thus fixing one of these combinations. In this case, all the modifications to the background evolution are governed by a single parameter  $s$ , defined in (19).

This parameter determines the evolution of the dark energy fluid in (21). At early times, the dark energy fluid is subdominant and its equation of state can be directly related to the equation of state of the matter-radiation fluid

$$1 + w_A \simeq -(1+w)s , \quad \rho_A \ll \rho . \quad (25)$$

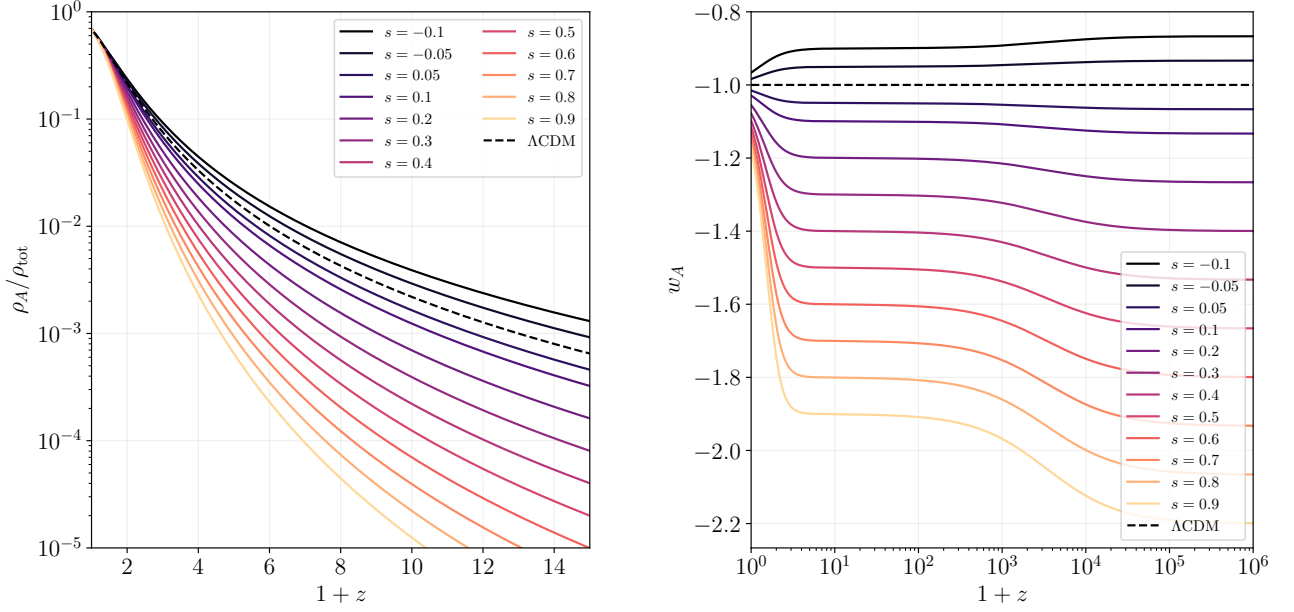


FIG. 1: (Left) Energy density of the Proca field normalized to the total density. (Right) Equation of state for different values of  $s$ . Notice that the equation of state is phantom for  $s > 0$ . In both plots, the dotted line represents a cosmological constant.

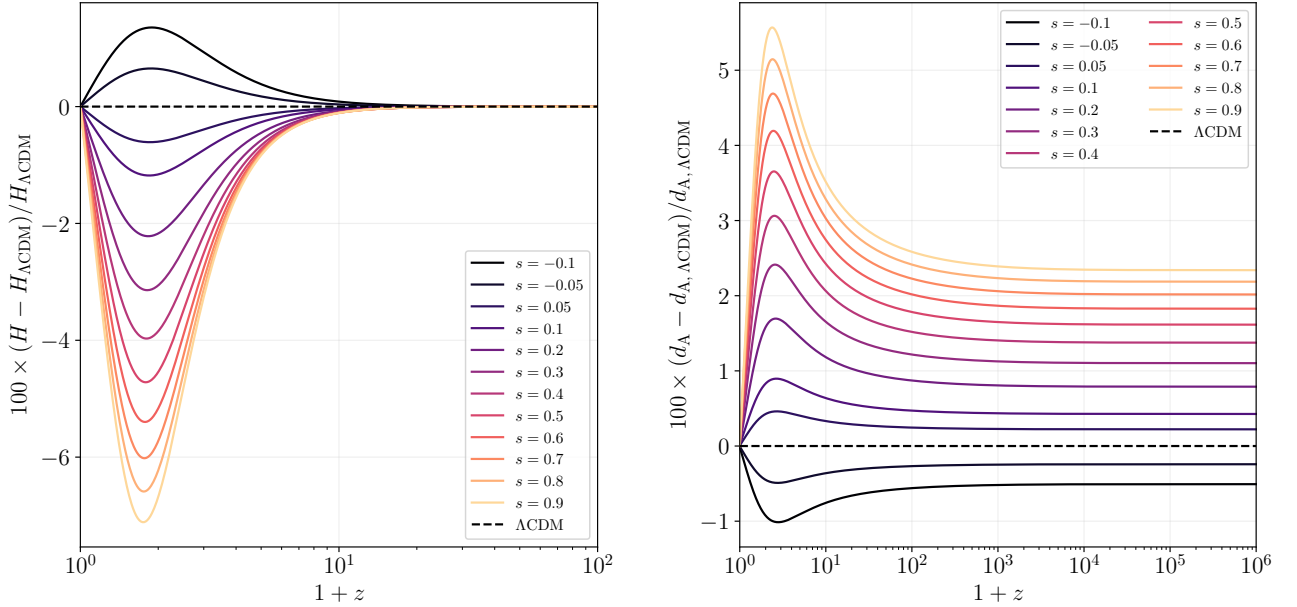


FIG. 2: Relative deviations in the Hubble parameter (Left) and the angular diameter distance (Right) with respect to the  $\Lambda$ CDM model.

In particular, for  $s = -1$  the fluid tracks exactly the evolution of the dominant component at the time. On the other hand, at late times, the fluid approaches the cosmological constant behaviour

$$w_A \simeq -1, \quad \rho_A \gg \rho. \quad (26)$$

It is important to notice that for  $s > 0$ , that will be our main concern, the dark energy is phantom-like, i.e.  $w_A < -1$ . Figure 1 contains the evolution of the energy density and the equation of state for different values of  $s$ . These modifications have a deep impact in the late-time evolution of the Hubble constant, as shown in Figure 2.

Modifications to the late-time expansion history can be directly tested with observations of (uncalibrated) SNe Ia. In Section V, we will use these observations, among other probes, to constrain the model. Changes in  $H(z)$  also affect the evolution of the perturbations and leave an imprint in the CMB and in the matter distribution. We will analyze these effects in the next section, after studying the evolution of the perturbations to the Proca field.

#### IV. PERTURBATIONS

In this section we consider a perturbed FLRW metric, taking only into account scalar perturbations

$$ds^2 = a^2(\tau) \left( - (1 + 2\Psi) d\tau^2 + 2\partial_i B d\tau dx^i + (\delta_{ij} - 2\Phi\delta_{ij} - \partial_i\partial_j E) dx^i dx^j \right). \quad (27)$$

Similarly, the scalar perturbations to the Proca field are

$$A^0 = \frac{1}{a}(\phi + \delta\phi), \quad (28a)$$

$$A^i = a^{-2}\delta^{ij}\partial_j\chi_V. \quad (28b)$$

In Appendix A we analyze the effect of a generic perturbation, proving that the vector modes can be neglected.

After plugging the Ansatz with perturbations into the vector field equations, one obtains

$$\begin{aligned} \mathcal{E}_0 &= \alpha \frac{k^2}{a^2} \left\{ a(\delta\phi + 2\Psi\phi) + \partial_\tau(\chi_V + a\phi B) \right\} + \frac{a\phi(\dot{\mathcal{H}} - \mathcal{H}^2)}{\dot{\phi}\mathcal{H}} G_{2,X}(\delta\phi + \Psi\phi) \\ &\quad + a\Psi G_{2,X}\phi + \frac{G_{2,X}}{3\mathcal{H}} \left( k^2\chi_V + a\phi(3\dot{\Phi} + k^2\dot{E}) \right) = 0, \end{aligned} \quad (29)$$

$$\begin{aligned} \frac{ik^i}{k^2} \mathcal{E}_i &= \frac{\alpha}{a^2} \left\{ \partial_\tau(a(\delta\phi + 2\Psi\phi)) + \partial_\tau^2(\chi_V + a\phi B) \right\} \\ &\quad - \frac{aG_{2,X}}{3\mathcal{H}}(\delta\phi + \Psi\phi) - \frac{G_{2,X}}{3\phi\mathcal{H}}\dot{\phi}(\chi_V + a\phi B) = 0. \end{aligned} \quad (30)$$

In a similar way, the energy-momentum tensor becomes this time

$$\begin{aligned} \delta T^0_0 &= \phi G_{2,X}(\delta\phi + \Psi\phi) - G_{2,X} \frac{\phi^2}{\mathcal{H}\dot{\phi}} (\dot{\mathcal{H}} - \mathcal{H}^2)(\delta\phi + \Psi\phi) - G_{2,X}\Psi\phi^2 \\ &\quad - \frac{\phi}{3a\mathcal{H}} G_{2,X} \left( k^2\chi_V + a\phi(3\dot{\Phi} + k^2\dot{E}) \right), \end{aligned} \quad (31)$$

$$ik^i \delta T^0_i = k^2 \frac{\phi G_{2,X}}{3\mathcal{H}} (\delta\phi + \Psi\phi), \quad (32)$$

$$\delta T^i_j = a^{-4}\delta^i_j \partial_\tau \left\{ \frac{a^4\phi}{3\mathcal{H}} G_{2,X}(\delta\phi + \Psi\phi) \right\} - \frac{1}{3\mathcal{H}} \phi\dot{\phi} G_{2,X}\Psi\delta^i_j. \quad (33)$$

We will adopt the usual definitions for the sources of the Einstein equations

$$\delta T^0_0 \equiv -\delta\rho, \quad ik^i \delta T^0_i \equiv (\rho_A + P_A)\theta_A, \quad \delta T^i_j \equiv \delta^i_j \delta P. \quad (34)$$

The system of equations can be greatly simplified by using the following set of dimensionless variables

$$\delta_\chi \equiv \frac{k(\chi_V + a\phi B)}{a\phi}, \quad (35a)$$

$$\delta_\phi \equiv \frac{k(\delta\phi + \Psi\phi)}{\dot{\phi}}, \quad (35b)$$

$$\mathcal{Z} \equiv -\frac{k^2\alpha\phi}{a^3\rho_A} \left( a(\delta\phi + 2\Psi\phi) + \partial_\tau(\chi_V + a\phi B) \right). \quad (35c)$$

With these definitions, the perturbed fluid variables are

$$\delta\rho_A + \frac{3\mathcal{H}}{k^2}(\rho_A + P_A)\theta_A = -\frac{\dot{\rho}_A}{\mathcal{H}}\frac{\dot{\phi}}{\phi}\left\{\left(\dot{\mathcal{H}} - \mathcal{H}^2\right)\frac{\delta\phi}{k} + \mathcal{H}\Psi + \frac{1}{3}\left(k\delta_\chi - k^2(B - \dot{E}) + 3\dot{\Phi}\right)\right\}, \quad (36a)$$

$$(\rho_A + P_A)\theta_A = k(1 + w_A)\rho_A\delta_\phi, \quad (36b)$$

$$\delta P_A = a^{-4}\partial_\tau\left(\frac{a^4}{k^2}(\rho_A + P_A)\theta_A\right) - \frac{\dot{\rho}_A}{3\mathcal{H}}\Psi. \quad (36c)$$

On the other hand, the equations of motion are

$$\mathcal{E}_0 = \frac{a}{\phi}\left\{-\rho_A\mathcal{Z} + \delta\rho_A + \frac{3\mathcal{H}}{k^2}(\rho_A + P_A)\theta_A\right\} = 0, \quad (37)$$

$$\frac{ik^i}{k^2}\mathcal{E}_i = \frac{a\rho_A}{k^2\phi}\left\{-\dot{\mathcal{Z}} + \left(\frac{\dot{\phi}}{\phi} - \frac{\dot{\rho}_A}{\rho_A} - 3\mathcal{H}\right)\mathcal{Z} + \frac{k}{3\mathcal{H}}\frac{\dot{\rho}_A}{\rho_A}(\delta_\chi + \delta_\phi)\right\} = 0. \quad (38)$$

The variable  $\delta_\phi$  can be obtained from (36a) and (37)

$$\left(\dot{\mathcal{H}} - \mathcal{H}^2\right)\delta_\phi = -k\mathcal{H}\frac{\dot{\phi}}{\phi}\frac{\rho_A}{\dot{\rho}_A}\mathcal{Z} + k\left(\frac{k^2}{3}(B - \dot{E}) - \dot{\Phi} - \mathcal{H}\Psi\right) - \frac{k^2}{3}\delta_\chi. \quad (39)$$

We can write a system for the two dynamical variables  $\delta_\chi$  and  $\mathcal{Z}$  using the definition (35c) and the equation of motion (38)

$$\dot{\delta}_\chi = -\left(\mathcal{H} + \frac{\dot{\phi}}{\phi}\right)\delta_\chi - \frac{a^2\rho_A}{\alpha\phi^2k}\mathcal{Z} - \frac{\dot{\phi}}{\phi}\delta_\phi - k\Psi, \quad (40)$$

$$\dot{\mathcal{Z}} = \left(\frac{\dot{\phi}}{\phi} - \frac{\dot{\rho}_A}{\rho_A} - 3\mathcal{H}\right)\mathcal{Z} + \frac{k}{3\mathcal{H}}\frac{\dot{\rho}_A}{\rho_A}(\delta_\chi + \delta_\phi). \quad (41)$$

### A. Dark energy model

We can particularize the results to the dark energy model that we considered in (16). From now on we will work in the Newtonian gauge, setting  $B = E = 0$ . We will also set the normalization  $\alpha = 1$  and measure the scalar field in Planck units  $M_{\text{P}}^{-1} = \sqrt{8\pi G}$ . Finally, we introduce one more variable redefinition, that is closely related to the velocity perturbation,

$$\mathcal{Q} \equiv -\frac{1}{p}\left(\mathcal{Z} + \frac{2ksp}{3\mathcal{H}}\delta_\chi\right). \quad (42)$$

The constraint (39) in terms of the new variable is

$$(1 + w_A)\delta_\phi = \frac{k}{3\mathcal{H}}\mathcal{Q} - \frac{2sk}{3\mathcal{H}^2}(\dot{\Phi} + \mathcal{H}\Psi). \quad (43)$$

After solving for the constraint, the system of equations for the evolution of the perturbations is reduced to

$$\dot{\mathcal{Q}} = -2\mathcal{H}\left(1 - \frac{3}{4}\mathcal{X}\right)\mathcal{Q} + \mathcal{H}\left(s\mathcal{R} + 3(1 + s\mathcal{R})c_A^2\right)\mathcal{Z} + \frac{2k^2s}{3\mathcal{H}}\Psi, \quad (44a)$$

$$\dot{\mathcal{Z}} = 3\mathcal{H}w_A\mathcal{Z} - \mathcal{H}\left(\frac{k^2}{3\mathcal{H}^2} + \frac{3}{2}\mathcal{X}\right)\mathcal{Q} + \frac{2k^2s}{3\mathcal{H}^2}(\dot{\Phi} + \mathcal{H}\Psi). \quad (44b)$$

where  $\mathcal{R}, \mathcal{X}$  have been defined in (23) and we have introduced

$$c_A^2 = (1 + s\mathcal{R})^{-1}p^{-1}\left\{\frac{2sp\mathcal{R}}{3\phi^2} + \frac{1}{3}(1 - sp\mathcal{R}) + \frac{1}{2}\left(1 + 2s - \frac{1}{p}\right)\mathcal{X}\right\}. \quad (45)$$

The sources of the Einstein equations are

$$(\rho_A + P_A)\theta_A = (1 + s\mathcal{R})^{-1} \left\{ \frac{k^2}{3\mathcal{H}} \rho_A \mathcal{Q} - s\mathcal{R}(\rho + P)\theta \right\} , \quad (46)$$

$$\delta\rho_A = \rho_A \mathcal{Z} - \frac{3\mathcal{H}}{k^2} (\rho_A + P_A)\theta_A . \quad (47)$$

Again,  $(\rho + P)\theta$  represents the momentum perturbation of all the fluids except the Proca field. As we can see, the perturbations  $\mathcal{Z}$  and  $\mathcal{Q}$  are directly related to the density and velocity perturbations of the dark energy fluid.

When solving for the evolution of perturbations we will restrict the parameter space, considering only models that satisfy the following consistency conditions.

- *Absence of ghost and gradient instabilities.* It was shown in [10] that these conditions amount to imposing

$$Q_A = \frac{3sp^2(1 + s\mathcal{R})\mathcal{H}^2\mathcal{R}}{(1 - sp\mathcal{R})^2 a^2 \phi^2} > 0 , \quad (48)$$

$$c_A^2 > 0 , \quad (49)$$

where  $c_A^2$  defined in (45) corresponds to  $c_S^2$  in [10] and  $Q_A$  corresponds to  $Q_S/a^3$  in the same reference. The first condition can be simply imposed by restricting to models where  $s > 0$ .

- *Absence of strong coupling.* Using the scaling relations (17) and (22) one can show that, in the  $\mathcal{R} \rightarrow 0$  limit,

$$Q_A \sim \frac{\mathcal{H}^2\mathcal{R}}{a^2\phi^2} \propto \mathcal{R}^{\frac{sp-1}{p(s+1)}} . \quad (50)$$

Since in the asymptotic past the dark energy fluid is subdominant,  $\mathcal{R} \rightarrow 0$ , in order to avoid strong coupling problems,  $Q_A \rightarrow 0$ , we must impose

$$sp = p_2 < 1 . \quad (51)$$

## B. Physical effects

The equations of motion (44a) and (44b), together with the sources (46) and (47), determine the evolution of the dark energy perturbations. In addition to the parameter  $s$  that determines the background evolution, the perturbations also depend on the parameters  $p$ , or  $p_2 = sp$ , and  $\phi_0$ .

In order to disentangle all the physical effects, we have studied two GP models. The first one contains only modifications at the background level and the results are represented in Figure 3. The second one contains both the effects on the background and the dark energy perturbations. The results are displayed in Figure 4, for a fixed value of  $s$ . The main physical processes at work can be summarized as follows.

- *Shifted acoustic scale.* The most noticeable effect in the right pannel of Figure 3 is a shift in the acoustic peaks. This is due to the modification of the background expansion history, that modifies the angular diameter distance

$$d_A = a \int_a^1 \frac{da'}{a'^2 H(a')} , \quad (52)$$

and hence the acoustic scale, that sets the angular position of the CMB peaks,

$$\theta_* = \frac{r_s(z_*)}{(1 + z_*)d_A(z_*)} , \quad (53)$$

where the comoving sound horizon at decoupling  $r_s(z_*)$  is not modified in our case. In particular it will be the phantom behaviour, with  $s > 0$ , that will help us to alleviate the Hubble tension.

- *Changes in the growth factor.* The evolution of the growth factor for matter perturbations is governed by, see (B12),

$$\ddot{D} + \mathcal{H}\dot{D} - 4\pi a^2 G_{\text{eff}} \rho_m D = 0 , \quad (54)$$



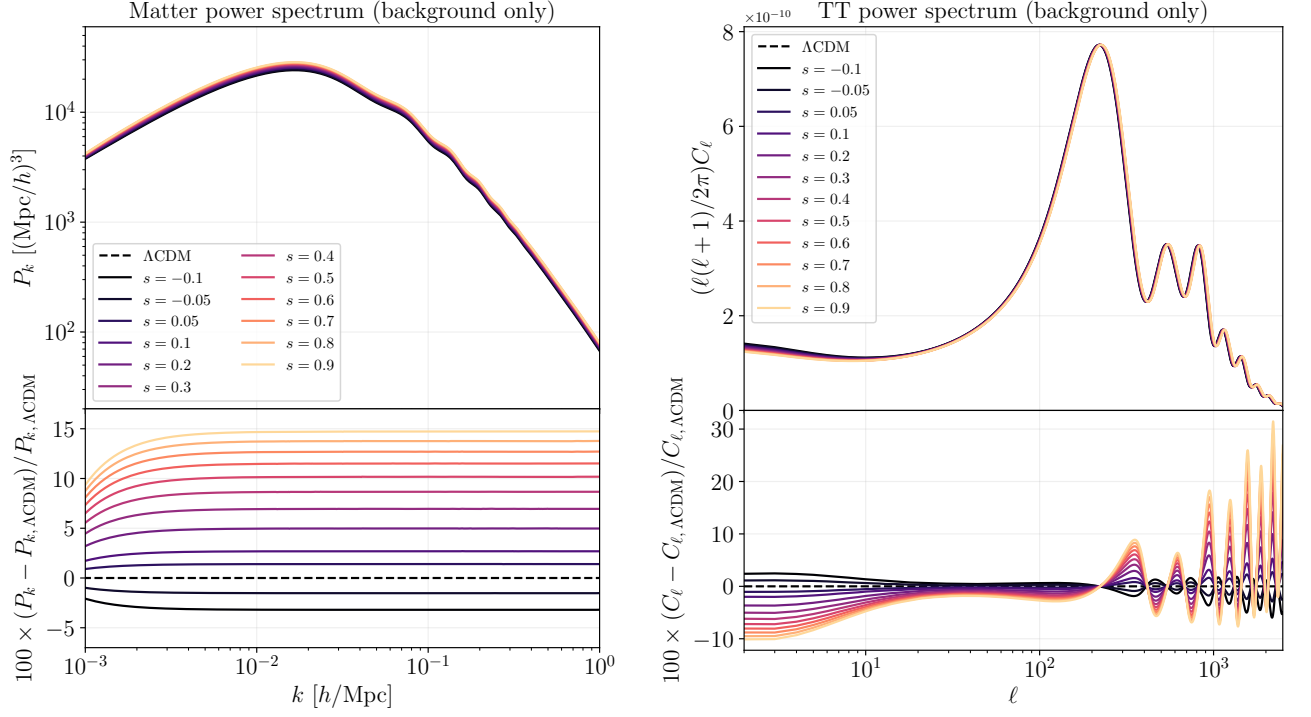


FIG. 3: Matter and temperature power spectra, including only the modifications to the background discussed in Section III. In the lower pannels we also show the relative deviations with respect to the  $\Lambda$ CDM result, depicted with a dotted line. As discussed in the main text, the modification of the expansion history has two key effects: (I) it changes the angular diameter distance to decoupling, shifting the CMB peaks, (II) it changes the growth factor, modifying the  $P_k$  amplitude and the CMB plateau.

where, in our case, the effective Newton constant is

$$\begin{aligned} \frac{G_{\text{eff}}}{G} &= 1 + \frac{s\mathcal{R}}{3(1+s\mathcal{R})c_A^2} \\ &= 1 + \frac{p_2\mathcal{R}}{1 - p_2\mathcal{R} + \frac{2p_2\mathcal{R}}{\phi^2} + \frac{3p_3}{p}\mathcal{X}}. \end{aligned} \quad (55)$$

Within  $\Lambda$ CDM,  $G_{\text{eff}} = G$  and the previous equation can be solved analitically giving the growing solution

$$D(a) \propto H(a) \int_0^a \frac{da'}{(a'H(a'))^3}. \quad (56)$$

In the Generalized Proca model, we have two different effects. In the first place, a modification of the expansion history  $H(a)$  leads to a modification of the growth factor and it affects the overall amplitude in the matter power spectrum. The reduction in  $H(a)$  that can be observed in Figure 2 then leads to an increase in the left pannel of Figure 3, and vice versa.

In the second place, the clustering properties of the dark energy fluid are encoded in  $G_{\text{eff}}$ . We see that, after taking into account the condition  $c_A^2 > 0$ , we always have  $G_{\text{eff}} > G$ . This effect further boosts the amplitude of the matter power spectrum on small scales in Figure 4.

- *ISW effect.* The late-time evolution of the gravitational potentials is affected in two ways. In the first place, if we consider only the modified background, the potentials are still decaying ( $\dot{\Phi} < 0$ ) as in  $\Lambda$ CDM but the overall ISW effect is suppressed. When we include the dark energy perturbations, the late-time evolution of the potentials is drastically modified and we can have both growing or decaying potentials at late times. As we will comment in Section VC, the case with growing potentials is strongly disfavoured by measurements of the temperature ISW-galaxy density cross correlation.

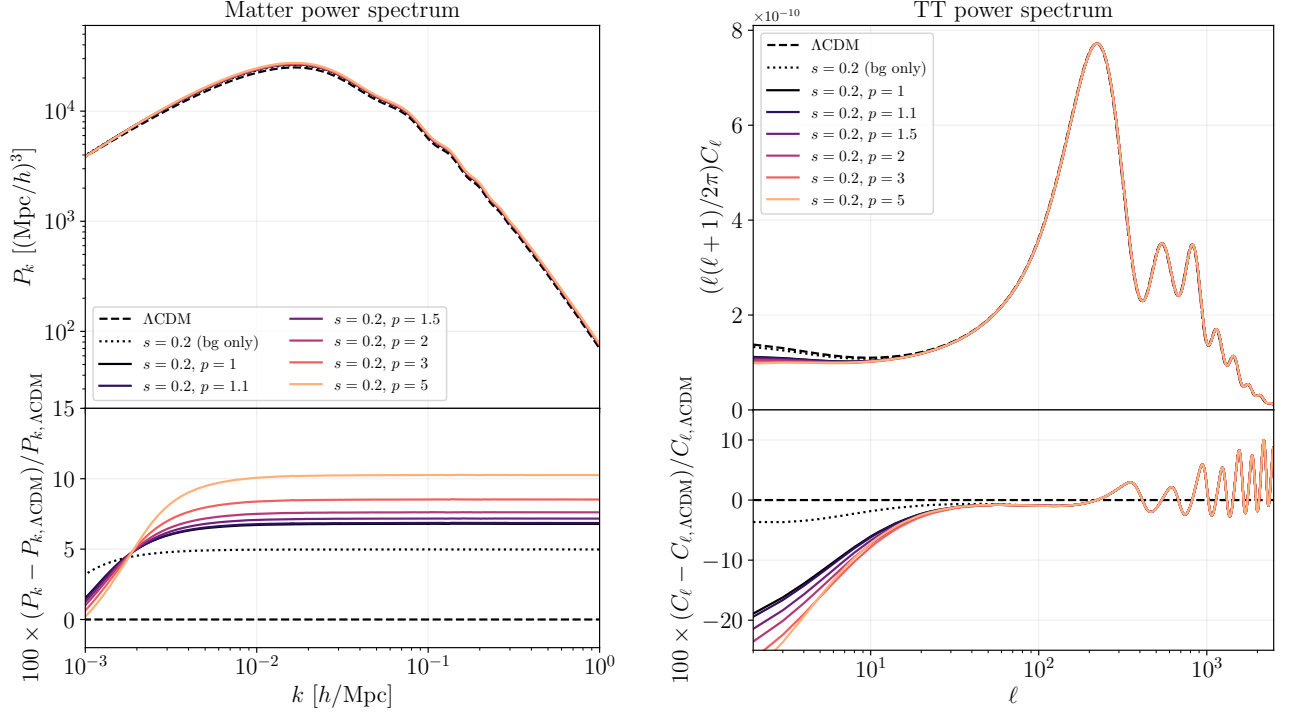


FIG. 4: Matter and temperature power spectra, including both the modified background and the perturbations. As discussed in the text, the effects observed can be traced back to the clustering properties of the dark energy fluid, that lead to a late-time evolution of the metric potentials.

## V. OBSERVATIONS

Once we have discussed the modifications to the background and perturbations, we will constrain the parameters of the GP model using cosmological observations and comparing with the  $\Lambda\text{CDM}$  predictions. We analyze the following models:

- **$\Lambda\text{CDM}$ .** We consider a flat  $\Lambda\text{CDM}$  model with fixed neutrino parameters  $N_{\text{eff}} = 3.046$  and  $\sum m_\nu = 0.06$  eV and the usual free parameters  $\{\Omega_b h^2, \Omega_{\text{cdm}} h^2, 100\theta_s, \log(10^{10} A_s), n_s, \tau_{\text{reio}}\}$ . See [4] for more details on this parameterization.
- **GP (bg only).** We consider a GP model without perturbations, taking only into account the modified expansion history, where the cosmological constant in the  $\Lambda\text{CDM}$  model is substituted by the Proca field acting as dark energy. On top of the  $\Lambda\text{CDM}$  parameters, this model includes an additional free parameter  $\{s\}$ , that modifies the dark energy equation of state (21). We choose a prior  $s \in [-0.1, 0.9]$ .
- **GP (bg+pert).** In this model we include both the modified background and the dark energy perturbations. On top of the parameters of the previous model, we have now two more free parameters  $\{\log_{10}(\phi_0), p_2\}$  that affect the evolution of the perturbations through their effects on the dark energy sound speed (45). We choose priors  $s \in [0, 0.9]$  and  $p_2 \in [0, 1]$ , consistent with the absence of ghosts and strong coupling problems. Additionally, we impose the stability condition  $c_A^2 > 0$ .

The sets of observations that we take into account are:

- **CMB.** We use the full temperature and polarization data (high- $\ell$  TTTEEE and low- $\ell$  TT and EE) from the latest *Planck* 2018 release [24]. We also include all the nuisance parameters.
- **SNe.** We use the Pantheon sample [25].
- **BAO.** We consider data from BOSS DR12 [26] and WiggleZ [27].
- **HST.** We use the measurement  $H_0 = 74.03 \pm 1.42$  from the SH0ES collaboration [3].

	CMB+SNe+BAO			CMB+SNe+BAO+HST		
	$\Lambda$ CDM	GP (bg)	GP (bg+pert)	$\Lambda$ CDM	GP (bg)	GP (bg+pert)
$100 \Omega_b h^2$	$2.244 \pm 0.014$	$2.237 \pm 0.014$	$2.246 \pm 0.015$	$2.255 \pm 0.013$	$2.239 \pm 0.015$	$2.248 \pm 0.015$
$\Omega_{\text{cdm}} h^2$	$0.1191 \pm 0.001$	$0.1202 \pm 0.0012$	$0.1194 \pm 0.0012$	$0.1179 \pm 0.00096$	$0.1202 \pm 0.0012$	$0.1195 \pm 0.0013$
$100 \theta_s$	$1.042 \pm 0.00029$	$1.042 \pm 0.00029$	$1.042 \pm 0.00029$	$1.042 \pm 0.00029$	$1.042 \pm 0.0003$	$1.042 \pm 0.0003$
$\log(10^{10} A_s)$	$3.047 \pm 0.017$	$3.046 \pm 0.016$	$3.040 \pm 0.016$	$3.048 \pm 0.017$	$3.045 \pm 0.017$	$3.040 \pm 0.016$
$n_s$	$0.9679 \pm 0.0039$	$0.9653 \pm 0.0041$	$0.9671 \pm 0.0042$	$0.9709 \pm 0.0038$	$0.9653 \pm 0.0042$	$0.967 \pm 0.0044$
$\tau_{\text{reio}}$	$0.05617^{+0.0076}_{-0.0084}$	$0.05437^{+0.0076}_{-0.0083}$	$0.05267 \pm 0.0078$	$0.05805^{+0.0074}_{-0.0087}$	$0.05406^{+0.0077}_{-0.0082}$	$0.05258^{+0.0076}_{-0.0079}$
$s$	–	$0.1049^{+0.043}_{-0.083}$	$0.07588^{+0.019}_{-0.076}$	–	$0.199^{+0.065}_{-0.083}$	$0.1613^{+0.066}_{-0.081}$
$p_2$	–	–	$0.6916^{+0.31}_{-0.085}$	–	–	$0.6887^{+0.31}_{-0.09}$
$\log_{10}(\phi_0)$	–	–	No constraint	–	–	No constraint
$\chi^2$	3804	3804	3794	3822	3814	3804
$\Delta\text{AIC}$	0	-2	4	0	6	12

TABLE I: Constraints on the free parameters of the models, considering two datasets: with and without the local distance measurement of the Hubble constant. We also include the minimum of the  $\chi^2$  and a comparison of the GP models to  $\Lambda$ CDM using the AIC, computed as  $\Delta\text{AIC} = \text{AIC}_{\Lambda\text{CDM}} - \text{AIC}_{\text{GP}}$ . The degeneracy in the  $p_2$ - $\phi_0$  plane is too large to obtain a credible confidence interval for  $\phi_0$ . As could be anticipated, both GP models can accomodate better the HST measurement of  $H_0$  providing a better fit than  $\Lambda$ CDM.

### A. Observational constraints

We perform four different runs for each model, combining CMB data with SNe, BAO and the direct  $H_0$  measurement. The main results of the fit are collected in Table I. Figures 5 and 6 show the marginalized contours for the two GP models, including the additional GP parameters and the most relevant cosmological variables. We also use the Akaike Information Criterion (AIC) [28, 29] to quantify the improvement of GP over the  $\Lambda$ CDM fit

$$\text{AIC} = 2N_{\text{param}} + \chi^2, \quad (57)$$

where  $N_{\text{param}}$  is the number of free parameters of the model and  $\chi^2 = -2 \log \mathcal{L}_{\text{max}}$  is computed from the maximum of the likelihood. This information criterion allows us to compare two competing models, penalizing models with more free parameters. For two different models  $A$  and  $B$ ,  $\text{AIC}_A - \text{AIC}_B > 5$  is widely regarded as a strong preference for model  $B$  [29].

In the Figures 5 and 6, we only show the results *without* HST data. As we can see, it is crucial to include SNe data, that constrains the equation of state of dark energy, in order to break the large degeneracy between  $s$  and  $H_0$ . Another way to break this degeneracy is to use the late-time measurements of  $H_0$  which would pull both  $s$  and  $H_0$  toward higher values.

Once we include the perturbations in the GP model, we find that the parameters  $p_2$  and  $\phi_0$  cannot be very well constrained. These two parameters affect the evolution of the perturbations through their effect on the sound speed and  $G_{\text{eff}}$ , see (55). From (55) we can see that in the limit  $\phi_0 \rightarrow 0$  we recover the  $\Lambda$ CDM behaviour, with  $G_{\text{eff}} \rightarrow G$ . However, the results in Figure 6 show that *large* values of  $\phi_0$  are actually favoured. We have checked that this is due to the fact that, in this region of parameter space, the suppression of the CMB plateau leads to a better fit to the low- $\ell$  TT data. As can be checked in Table I, this model improves the  $\Lambda$ CDM fit even without including the HST observation. However, also in this region of parameter space, the late-time growth of the metric potentials may result in a strong disagreement with the observations of temperature ISW and galaxy density cross-correlations, not included in our analysis. We will discuss this matter further in Section V C.

### B. $H_0$ tension

As we have already discussed, the phantom-like equation of state of GP models modifies the angular diameter distance to the last-scattering surface, shifting the CMB peaks and favouring a large  $H_0$ . Other models of dark energy with phantom-like equations of state, like scalar Galileons [9, 30], present a similar behaviour. When comparing with CMB observations, this effect introduces a large degeneracy between the parameter  $s$ , that governs the dark energy equation of state, and  $H_0$ . Adding external data is crucial to break this degeneracy.

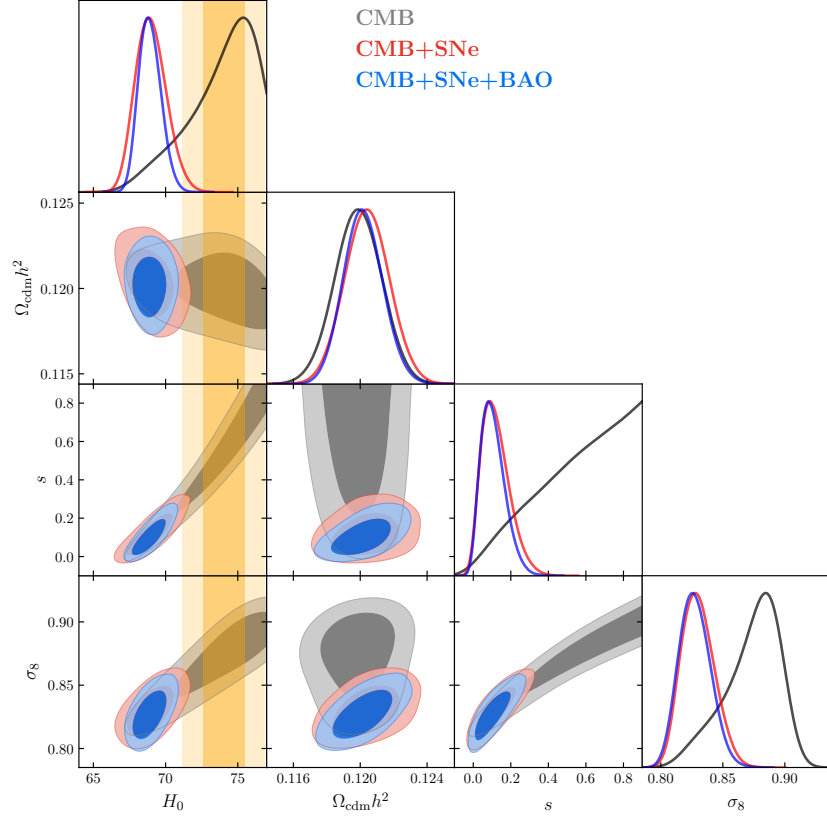


FIG. 5: 68% and 95% CL contours for the GP (bg only) model. The vertical bands are the 68% and 95% CL limits from the local distance measurement of the Hubble constant [3].

	CMB+SNe+BAO			CMB+SNe+BAO+HST		
	$\Lambda$ CDM	GP (bg)	GP (bg+pert)	$\Lambda$ CDM	GP (bg)	GP (bg+pert)
$\Omega_m$	$0.3077 \pm 0.006$	$0.3003^{+0.0074}_{-0.0071}$	$0.2991 \pm 0.007$	$0.3005^{+0.0054}_{-0.0057}$	$0.2894^{+0.0062}_{-0.0067}$	$0.2889^{+0.0063}_{-0.0066}$
$\sigma_8$	$0.8088^{+0.0072}_{-0.0076}$	$0.8273 \pm 0.013$	$0.8374 \pm 0.012$	$0.8059^{+0.0072}_{-0.0077}$	$0.8397 \pm 0.013$	$0.8477 \pm 0.013$
$S_8$	$0.819 \pm 0.013$	$0.8276 \pm 0.014$	$0.8362 \pm 0.014$	$0.8066 \pm 0.013$	$0.8245 \pm 0.013$	$0.8319 \pm 0.014$
$H_0$	$67.83 \pm 0.45$	$68.91^{+0.69}_{-0.86}$	$68.88^{+0.62}_{-0.8}$	$68.38 \pm 0.43$	$70.21 \pm 0.76$	$70.1 \pm 0.76$
$H_0$ tension	$4.2\sigma$	$3.2\sigma$	$3.2\sigma$	$3.8\sigma$	$2.4\sigma$	$2.4\sigma$

TABLE II: Constraints on some derived parameters, considering two datasets: with and without the local distance measurement of the Hubble constant. The Hubble tension is evaluated approximating the 1d posterior on  $H_0$  as Gaussian and comparing with the local value  $H_0 = 74.03 \pm 1.42$  from the SH0ES collaboration [3].

One possibility is to use a direct measurement of the Hubble constant, like the local value from the SH0ES collaboration [3]. This was the approach taken in [11]. However, in order to address the so-called  $H_0$  tension without imposing this prior, we have chosen to break this degeneracy combining CMB with SNe and BAO data. When we include the HST measurement as well,  $H_0$  is pulled toward larger values. The most relevant results for the Hubble tension are collected in Table II and in Figure 7.

It is important to notice that GP models naturally prefer higher values of  $H_0$ , even without using the HST observation. In this way, GP can fit CMB, BAO and SNe data as successfully as  $\Lambda$ CDM (or even better) while reducing the Hubble tension by  $1\sigma$ . In addition, if we include HST data, the tension is reduced to  $2.4\sigma$ .

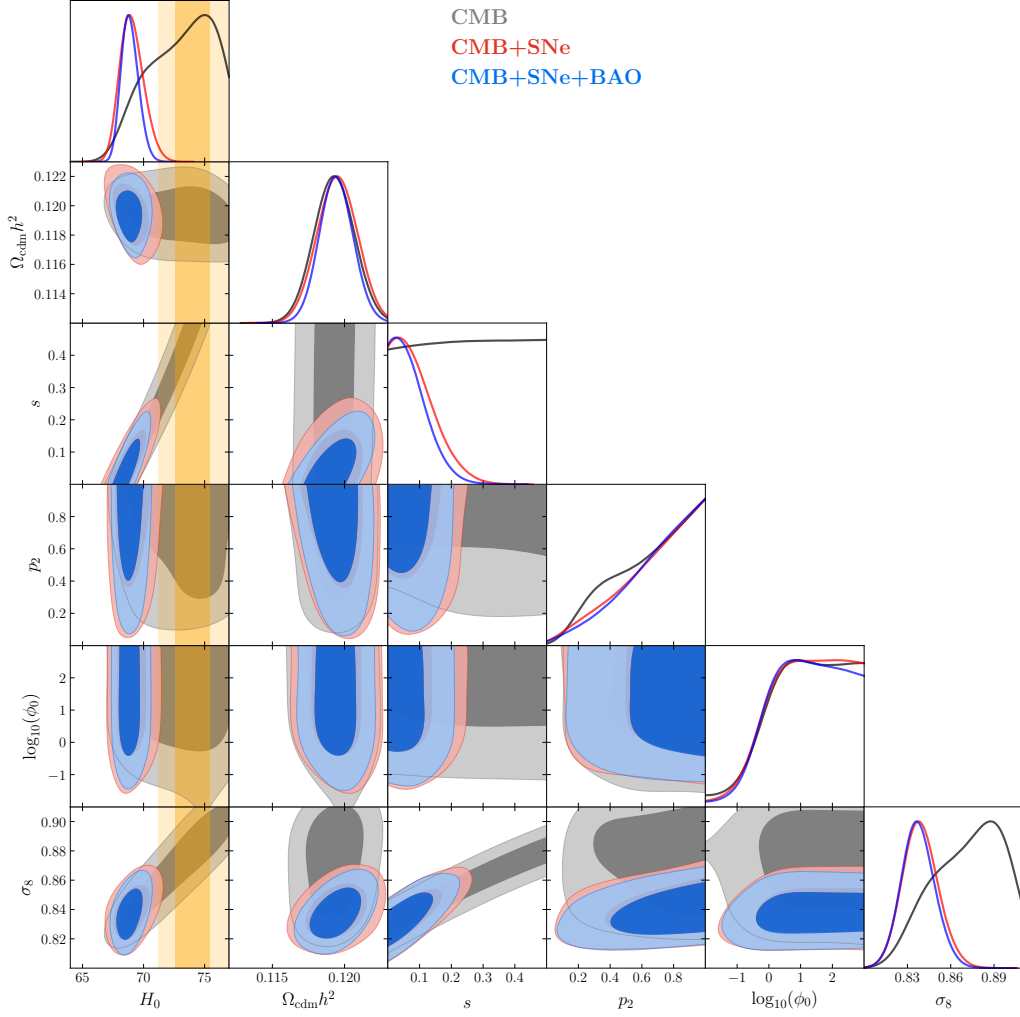


FIG. 6: 68% and 95% CL contours for the GP (bg+pert) model. The vertical bands are the 68% and 95% CL limits from the local distance measurement of the Hubble constant [3].

### C. Complementary observations: $\sigma_8$ and ISW effect

The novel clustering properties of the dark energy fluid can produce, for some combinations of parameters, a late-time growth (deepening) of the gravitational potentials. This leads to an increased clustering amplitude, i.e. larger  $\sigma_8$ , and to an ISW effect with the opposite sign, as compared with  $\Lambda$ CDM. These are two common side effects of late-time solutions to the Hubble tension based on dark energy. While relieving the  $H_0$  tension, we can spoil the fit to other observations, e.g. increasing the  $\sigma_8$  tension.

The consistency of the  $\sigma_8$  value inferred from the CMB and the one measured by weak lensing and galaxy clustering surveys has been a matter of debate for years, and is usually known as the  $\sigma_8$  tension. On the one hand, the latest *Planck* value (including CMB lensing and BAO data) for the parameter  $S_8 \equiv \sigma_8 \sqrt{\Omega_m/0.3}$  is  $S_8 = 0.825 \pm 0.011$  (68% CL) [4]. On the other hand, the latest measurements by DES Y1 ( $S_8 = 0.773^{+0.026}_{-0.020}$ ) [31] and KiDS-1000 ( $S_8 = 0.766^{+0.020}_{-0.014}$ ) [32] are consistently lower (see Fig. 5 in [32] for a full list of recent measurements).

Even though the different collaborations do not seem to agree about the consistency of the results, i.e. about the existence of a ‘tension’, a general lesson to be learnt is that any  $S_8$  value significantly higher than the *Planck* measurement should be strongly disfavoured. It would then seem worrying that in the GP model we obtain slightly larger values for  $S_8$ , see Table II, but there are at least two caveats. First, the constraints from galaxy surveys depend on the underlying cosmological model. For instance, the DES collaboration also reports the measurement  $S_8 = 0.782^{+0.036}_{-0.024}$  in a dark energy model with a constant equation of state ( $w$ CDM). To perform a fair comparison with the GP model, one would need to take into account the modified background. The second caveat is that, to

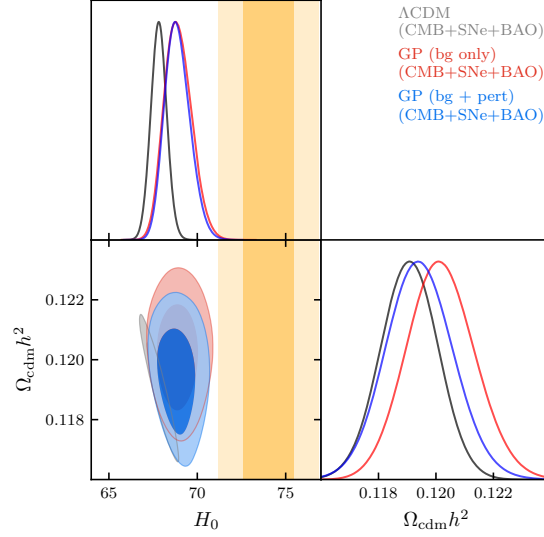


FIG. 7: Comparison of the  $\Lambda$ CDM and GP models (with 68% and 95% CL). Again, the vertical band is the HST measurement of  $H_0$  [3]. Notice that in this plot, the HST has *not* been included in the analysis. Even without the HST prior, GP models predict a larger  $H_0$ . Once we include HST, the fit is pulled towards even larger values of  $H_0$ , close to the local value.

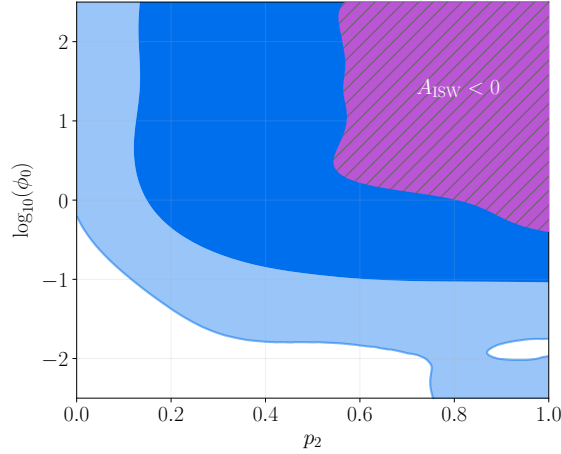


FIG. 8: 95% and 99% CL contour on the GP parameters  $\phi_0$ - $p_2$ . These two parameters only affect the evolution of the perturbations, modifying the sound speed of dark energy. The region with  $A_{\text{ISW}} < 0$  is most likely excluded by measurements of the temperature ISW-galaxy density cross-correlation.

address the consistency of measurements, it is important to analyze the multidimensional posterior. Besides decreasing  $S_8$ , another generic feature of weak lensing surveys is to predict lower values for  $\Omega_m$ , thus displacing the minimum in the  $\Omega_m$ - $S_8$  plane. While the GP model increases slightly the tension in one direction (increasing  $S_8$ ) it also predicts lower values for  $\Omega_m$ , reducing the tension in that direction. All these effects should be taken into account when comparing with LSS clustering data.

The temperature ISW effect depends on the (integrated) time evolution of the gravitational potentials. The low- $\ell$  CMB plateau is affected by modifications to the ISW term, but it is largely insensitive to its sign. This sign carries important information, e.g. it can reveal whether the potentials are growing or decaying, and it can be recovered from the cross-correlation of CMB temperature data and galaxy density observations [9, 33–35]. Different observations are available and have been fruitfully applied to test dark energy [36–38]. In particular, ISW observations have already been used to constrain our GP model [37] but without using the full CMB data. The results of [37] show that small values of  $\phi_0$  are preferred by these observations.

A precise comparison with ISW data would require a dedicated analysis. In this work, we only estimate the sign

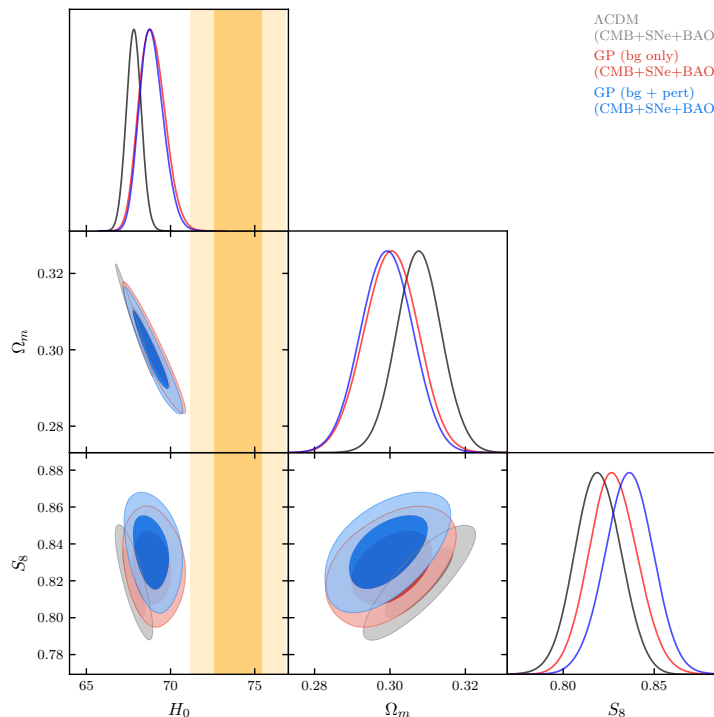


FIG. 9: Comparison of the  $\Lambda$ CDM and GP models (with 68% and 95% CL). We use the variable  $S_8 \equiv \sigma_8 \sqrt{\Omega_m/0.3}$ , that is very precisely constrained by weak lensing surveys. On top of predicting a higher  $H_0$  value, GP models also favour lower values of  $\Omega_m$ .

of the ISW effect, by adding all the cross-correlation multipoles,  $A_{\text{ISW}} \equiv \sum_{\ell} C_{\ell}^{Tg}$ . Combinations of parameters that yield a negative cross-correlation ( $A_{\text{ISW}} < 0$ ) must be strongly disfavoured. In Figure 8 we show the  $2\sigma$  and  $3\sigma$  contours of the two parameters related to the clustering properties of the model,  $\phi_0$  and  $p_2$ . In agreement with [37], we observe that a large region of parameter space, with large  $\phi_0$  values, is ruled out by ISW observations. The combination of the full CMB data, that favours large  $\phi_0$  values as we show in this work, and temperature ISW-galaxy density cross-correlation, that favours small  $\phi_0$  values as shown in [37], could then be used to break the degeneracy and tightly constrain  $\phi_0$ .

## VI. SUMMARY AND CONCLUSIONS

In this work, we have studied in detail the phenomenology of a simple Generalized Proca model for dark energy. After comparing with CMB, BAO and SNe observations (without imposing a  $H_0$  prior) we have showed that it can relieve the Hubble tension by about  $1\sigma$ .

This class of models can reduce the Hubble tension mainly because of the phantom-like behaviour of dark energy, in a similar way to scalar Galileon models. The modified expansion history reduces the angular diameter distance to the last-scattering surface, shifting the CMB peaks and introducing a high degeneracy with  $H_0$ . In this scenario, if we impose a prior in  $H_0$ , like in [11], a high value is trivially preferred. However, in our case, instead of using the local  $H_0$  measurements, we have broken this degeneracy in the CMB data using SNe data, that can constrain the equation of state of dark energy. We have shown that, even without the local  $H_0$  prior, the GP model naturally favours higher values of  $H_0$ , easing the Hubble tension.

The modified background is the main responsible for relieving the Hubble tension, but we have also studied the perturbations in the model. Both the novel clustering properties of dark energy and the modified background produce a late-time evolution of the metric potentials that modify the ISW effect. This produces a modification on the CMB spectrum at low  $\ell$ , i.e. the SW plateau. In particular, once we include the perturbations, the suppression of the SW plateau can lead to a better fit to CMB data.

Finally, we checked the consistency of our results with complementary observations from LSS. A well-known side effect of dark-energy solutions to the Hubble tension is a potential disagreement with LSS observations. The GP

model predicts a slightly larger value for  $\sigma_8$ , while also reducing the value of  $\Omega_m$  so the tension on the  $\sigma_8$ - $\Omega_m$  plane would have to be properly studied, and can also potentially produce an ISW-galaxy density cross-correlation with the wrong sign. Some of these aspects have been previously studied in [37], where the authors constrained the GP model using ISW measurements, but only using reduced CMB information. It was shown that the GP model is compatible with ISW observations in some region of parameter space.

Further study in this direction would involve extending our analysis to include clustering data and ISW measurements. The compromise between achieving a better fit to CMB low- $\ell$ , as shown in this work, while simultaneously agreeing with ISW observations, as in [37], would then allow us to confidently constrain all the parameters of this model.

### Acknowledgments

LH is supported by funding from the European Research Council (ERC) under the European Unions Horizon 2020 research and innovation programme grant agreement No 801781 and by the Swiss National Science Foundation grant 179740.

### Appendix A: General perturbations

In this appendix we present the full equations of motion and the energy-momentum tensor, for a generic metric and field perturbation and before applying the equations of motion at the background level. We start with a general perturbed FLRW metric, that can be written as

$$ds^2 = a^2(\tau) \left( - (1 - A) d\tau^2 + 2B_i d\tau dx^i + (\delta_{ij} + H_{ij}) dx^i dx^j \right), \quad (A1)$$

and we parameterize the perturbations to the Proca field as

$$A^0 = \frac{1}{a}(\phi + \delta\phi), \quad (A2a)$$

$$A^i = a^{-2} \delta^{ij} (\partial_j \chi_V + E_j), \quad (A2b)$$

where  $\delta\phi$  and  $\chi_V$  are scalar perturbations and  $E_i$  is the transverse part of the vector field, i.e. a vector perturbation.

*Equations of motion.*

$$\begin{aligned} \mathcal{E}_0 = & \alpha \frac{k^2}{a^2} \left\{ a\delta\phi + \dot{\chi}_V - a \frac{i\hat{k}^i}{k} B_i \dot{\phi} - a\phi \left[ A + \frac{i\hat{k}^i}{k} (\dot{B}_i + \mathcal{H}B_i) \right] \right\} \\ & + \left( \delta\phi - \frac{1}{2}\phi A \right) \left\{ aG_{2,X} + aG_{2,XX}\phi^2 + 3\mathcal{H}G_{3,XX}\phi^3 + 6\mathcal{H}G_{3,X}\phi \right\} \\ & - \frac{1}{2}aAG_{2,X}\phi - a^{-1}G_{3,X}\phi \left( k^2\chi_V - \frac{1}{2}a\phi\dot{H}_i^i \right) = 0, \end{aligned} \quad (A3)$$

$$\begin{aligned} \mathcal{E}_i = & -\frac{\alpha}{a^2} \left\{ a i k_i (\delta\dot{\phi} - \phi\dot{A} + \mathcal{H}\delta\phi - \mathcal{H}\phi A - \dot{\phi}A) + a\phi\ddot{B}_i + 2a\dot{B}_i(\dot{\phi} + \mathcal{H}\phi) - a\phi k_i k^j B_j \right. \\ & \left. + aB_i (\ddot{\phi} + 2\mathcal{H}\dot{\phi} (\mathcal{H} + \mathcal{H}^2 + k^2) \phi) + i k_i \ddot{\chi}_V + \ddot{E}_i + k^2 E_i \right\} \\ & - G_{2,X} (i k_i \chi_V + E_i + a\phi B_i) \\ & - G_{3,X} \left\{ i k_i \phi \left( \delta\phi - \frac{1}{2}\phi A \right) + a^{-1} (\dot{\phi} + 3\mathcal{H}\phi) (i k_i \chi_V + E_i + a\phi B_i) \right\} = 0. \end{aligned} \quad (A4)$$

*Energy-momentum tensor.*

$$\begin{aligned} T^0_0 = & -\frac{\phi}{a} \left( \delta\phi - \frac{1}{2}\phi A \right) (aG_{2,X} + aG_{2,XX}\phi^2 + 9\mathcal{H}G_{3,X}\phi + 3\mathcal{H}G_{3,XX}\phi^3) \\ & - \frac{3\mathcal{H}}{2a} AG_{3,X}\phi^3 + \frac{\phi^2}{a^2} G_{3,X} \left( k^2\chi_V - \frac{1}{2}a\phi\dot{H}_i^i \right), \end{aligned} \quad (A5)$$



$$T_i^0 = \frac{\phi}{a^2} (aG_{2,X} + 3\mathcal{H}\phi G_{3,X}) (ik_i\chi_V + E_i + a\phi B_i) + \frac{ik_i}{a} G_{3,X} \phi^2 \left( \delta\phi - \frac{1}{2}\phi A \right), \quad (\text{A6})$$

$$T_j^i = -\frac{\phi}{a} \delta_j^i \left\{ \phi G_{3,X} \left( \delta\dot{\phi} - \frac{1}{2}\phi\dot{A} \right) - \left( \delta\phi - \frac{1}{2}\phi A \right) \left( aG_{2,X} - 2\dot{\phi}G_{3,X} - \dot{\phi}G_{3,XX}\phi^2 \right) \right\}. \quad (\text{A7})$$

It is important to notice that once we apply the equations of motion at the background level, the vector component of  $T_i^0$  vanishes. This implies that the vector field does not source vorticity in the Einstein equations and thus it is purely decaying and negligible as in  $\Lambda$ CDM (in agreement with [21]). Once we apply the equations of motion at the background level, (10a) and (13), the results of the main text can be recovered setting

$$A = -2\Psi, \quad (\text{A8})$$

$$B_i = ik_i B, \quad (\text{A9})$$

$$H_{ij} = -2\Phi\delta_{ij} - 2k_ik_j E. \quad (\text{A10})$$

## Appendix B: Super- and sub-Hubble analysis

In this appendix we will use  $N = \log(a)$  as time variable, and denote  $' \equiv \partial_N$ . The energy-momentum tensor conservation for a generic fluid leads to the continuity and Euler equations

$$\Delta' = 3w\Delta - \frac{k}{\mathcal{H}} \left\{ 1 + \frac{3\mathcal{H}}{k} \left( 1 - \frac{\mathcal{H}'}{\mathcal{H}} \right) \right\} u - 4\sigma + (1+w)(\Phi' + \Psi), \quad (\text{B1a})$$

$$u' = -u - 3(c_s^2 - w)u - \frac{kc_s^2}{\mathcal{H}} \Delta - \frac{4k}{3\mathcal{H}} \sigma + \frac{k}{\mathcal{H}} (1+w)\Psi, \quad (\text{B1b})$$

expressed in terms of the gauge-invariant density perturbation  $\Delta$  and the velocity perturbation  $u$ , that are related to the usual energy density and velocity divergence as

$$\Delta \equiv \delta + \frac{3\mathcal{H}(1+w)\theta}{k^2}, \quad u \equiv \frac{1}{k}(1+w)\theta. \quad (\text{B2})$$

The Einstein equations can be written as

$$\Phi = -\frac{3\mathcal{H}^2}{2k^2} (\mathcal{R}\mathcal{Z} + \tilde{\mathcal{R}}\Delta), \quad (\text{B3a})$$

$$\Phi - \Psi = \frac{6\mathcal{H}^2}{k^2} \mathcal{R}\sigma, \quad (\text{B3b})$$

$$\Phi' + \Psi = \frac{3\mathcal{H}}{2k(1+s\mathcal{R})} \left( \frac{k}{3\mathcal{H}} \mathcal{R}\mathcal{Q} + \tilde{\mathcal{R}}u \right). \quad (\text{B3c})$$

For simplicity, we will restrict ourselves to perfect fluids,  $\sigma = 0$ , and  $c_s^2 = w = \text{const.}$ . Using the Einstein equations (B3), we can combine the equations for the fluid (B1) and for the Proca field (44) into two coupled second-order differential equations for the gauge-invariant density perturbations  $\mathcal{Z}$  and  $\Delta$ . In order to grasp the behaviour of the system, we will study both the super-Hubble ( $k \ll \mathcal{H}$ ) and sub-Hubble ( $k \gg \mathcal{H}$ ) limits.

### 1. Super-Hubble limit

In the super-Hubble limit, the evolution of  $\mathcal{Z}$  decouples from  $\Delta$ , i.e.  $\Delta$  does not appear in the equation for  $\mathcal{Z}'$ . However, as we will see later, the super-Hubble behaviour of  $\mathcal{Z}$  is not particularly relevant since there is an attractor solution in the sub-Hubble regime. The full expressions in this regime are not very illuminating, so we will focus on two limiting cases. First, if the Proca field is subdominant ( $\mathcal{R} \rightarrow 0$ ) we have

$$\mathcal{Z}'' = -5 \left( 1 - \frac{3(1+w)(1-2s)}{10} \right) \mathcal{Z}' - 6 \left\{ 1 + (1+w) \left( s + \frac{3}{4}(c_A^2 - 1 - s(1+w)) \right) \right\} \mathcal{Z} + \mathcal{O}\left(\frac{k}{\mathcal{H}}\right), \quad (\text{B4})$$

$$\Delta'' = -\frac{9w-1}{2} \Delta' - \frac{3}{2}(w-1)(1+3w)\Delta + \mathcal{O}\left(\frac{k}{\mathcal{H}}\right). \quad (\text{B5})$$

In the opposite limit, on the de Sitter attractor  $\mathcal{R} \rightarrow 1$ , we have

$$\mathcal{Z}'' = -(15 + 9w)\mathcal{Z}' - (8 + 3w)\mathcal{Z} + \mathcal{O}\left(\frac{k}{\mathcal{H}}\right) , \quad (\text{B6})$$

$$\Delta'' = (3w - 2)\Delta' + 6w\Delta - 3(1 + w)\mathcal{Z}' + \frac{3}{2}(1 + w)(3c_A^2 - 5)\mathcal{Z} + \mathcal{O}\left(\frac{k}{\mathcal{H}}\right) . \quad (\text{B7})$$

## 2. Sub-Hubble limit

To lowest order in the sub-Hubble limit we have

$$\mathcal{Z}'' = -\frac{k^2}{\mathcal{H}^2} \left\{ c_A^2 \mathcal{Z} - \frac{s(1 + 3w)}{3(1 + s\mathcal{R})} \tilde{\mathcal{R}}\Delta \right\} + \mathcal{O}(1) , \quad (\text{B8})$$

$$\begin{aligned} \Delta'' = & -\left(1 - 3w + \frac{\mathcal{H}'}{\mathcal{H}}\right) \Delta' + \left(1 + 3w - (1 - 3w)\frac{\mathcal{H}'}{\mathcal{H}}\right) \Delta - \frac{k^2}{\mathcal{H}^2} w\Delta \\ & + \frac{3}{2}(1 + w)(1 + 3c_A^2)\mathcal{Z} + \mathcal{O}\left(\frac{\mathcal{H}}{k}\right) . \end{aligned} \quad (\text{B9})$$

In this regime we can approximate

$$\mathcal{R}\mathcal{Z} \simeq (1 + 3w)\mathcal{F}\tilde{\mathcal{R}}\Delta , \quad \mathcal{F} \equiv \frac{s\mathcal{R}}{3(1 + s\mathcal{R})c_A^2} . \quad (\text{B10})$$

Substituting into the equation for  $\Delta$

$$\Delta'' = -\left(1 - 3w + \frac{\mathcal{H}'}{\mathcal{H}}\right) \Delta' + \frac{3}{2}\tilde{\mathcal{R}}(1 + 3w)(1 + w)(1 + \mathcal{F})\Delta + 6\frac{\mathcal{H}'}{\mathcal{H}}w\Delta - \frac{k^2}{\mathcal{H}^2}w\Delta . \quad (\text{B11})$$

In particular, in the late Universe  $w = 0$  and  $\Delta$  is the total matter density perturbation. In this case, we obtain the usual expression for the matter growth function

$$\Delta'' = -\left(1 + \frac{\mathcal{H}'}{\mathcal{H}}\right) \Delta' + \frac{4\pi G_{\text{eff}} a^2}{\mathcal{H}^2} \rho_m \Delta , \quad (\text{B12})$$

where

$$\frac{G_{\text{eff}}}{G} = 1 + \mathcal{F} . \quad (\text{B13})$$

- 
- [1] J. B. Jiménez, L. Heisenberg, and T. S. Koivisto, *Universe* **5**, 173 (2019), 1903.06830.
  - [2] L. Heisenberg, *Phys. Rept.* **796**, 1 (2019), 1807.01725.
  - [3] A. G. Riess, S. Casertano, W. Yuan, L. M. Macri, and D. Scolnic, *Astrophys. J.* **876**, 85 (2019), 1903.07603.
  - [4] N. Aghanim et al. (Planck) (2018), 1807.06209.
  - [5] A. Nicolis, R. Rattazzi, and E. Trincherini, *Phys. Rev. D* **79**, 064036 (2009), 0811.2197.
  - [6] C. Deffayet, G. Esposito-Farese, and A. Vikman, *Phys. Rev. D* **79**, 084003 (2009), 0901.1314.
  - [7] G. W. Horndeski, *Int. J. Theor. Phys.* **10**, 363 (1974).
  - [8] A. Banerjee, H. Cai, L. Heisenberg, E. Ó. Colgáin, M. Sheikh-Jabbari, and T. Yang (2020), 2006.00244.
  - [9] J. Renk, M. Zumalacárregui, F. Montanari, and A. Barreira, *JCAP* **10**, 020 (2017), 1707.02263.
  - [10] A. De Felice, L. Heisenberg, and S. Tsujikawa, *Phys. Rev. D* **95**, 123540 (2017), 1703.09573.
  - [11] A. De Felice, C.-Q. Geng, M. C. Pookkillath, and L. Yin, *JCAP* **08**, 038 (2020), 2002.06782.
  - [12] D. Blas, J. Lesgourgues, and T. Tram, *JCAP* **07**, 034 (2011), 1104.2933.
  - [13] B. Audren, J. Lesgourgues, K. Benabed, and S. Prunet, *JCAP* **02**, 001 (2013), 1210.7183.
  - [14] T. Brinckmann and J. Lesgourgues, *Phys. Dark Univ.* **24**, 100260 (2019), 1804.07261.
  - [15] A. Lewis (2019), 1910.13970.
  - [16] L. Heisenberg, *JCAP* **05**, 015 (2014), 1402.7026.
  - [17] E. Allys, P. Peter, and Y. Rodriguez, *JCAP* **02**, 004 (2016), 1511.03101.

- [18] J. Beltran Jimenez and L. Heisenberg, Phys. Lett. B **757**, 405 (2016), 1602.03410.
- [19] G. Tasinato, JHEP **04**, 067 (2014), 1402.6450.
- [20] A. De Felice, L. Heisenberg, R. Kase, S. Mukohyama, S. Tsujikawa, and Y.-l. Zhang, JCAP **06**, 048 (2016), 1603.05806.
- [21] A. De Felice, L. Heisenberg, R. Kase, S. Mukohyama, S. Tsujikawa, and Y.-l. Zhang, Phys. Rev. D **94**, 044024 (2016), 1605.05066.
- [22] J. Chagoya, G. Niz, and G. Tasinato, Class. Quant. Grav. **34**, 165002 (2017), 1703.09555.
- [23] L. Heisenberg, R. Kase, M. Minamitsuji, and S. Tsujikawa, JCAP **08**, 024 (2017), 1706.05115.
- [24] N. Aghanim et al. (Planck) (2019), 1907.12875.
- [25] D. Scolnic et al., Astrophys. J. **859**, 101 (2018), 1710.00845.
- [26] S. Alam et al. (BOSS), Mon. Not. Roy. Astron. Soc. **470**, 2617 (2017), 1607.03155.
- [27] E. A. Kazin et al., Mon. Not. Roy. Astron. Soc. **441**, 3524 (2014), 1401.0358.
- [28] H. Akaike, IEEE transactions on automatic control **19**, 716 (1974).
- [29] A. R. Liddle, Mon. Not. Roy. Astron. Soc. **377**, L74 (2007), astro-ph/0701113.
- [30] A. Barreira, B. Li, C. Baugh, and S. Pascoli, JCAP **08**, 059 (2014), 1406.0485.
- [31] T. Abbott et al. (DES), Phys. Rev. D **98**, 043526 (2018), 1708.01530.
- [32] C. Heymans et al. (KiDS) (2020), 2007.15632.
- [33] R. Bean and O. Dore, Phys. Rev. D **69**, 083503 (2004), astro-ph/0307100.
- [34] W. Hu and R. Scranton, Phys. Rev. D **70**, 123002 (2004), astro-ph/0408456.
- [35] M. Ballardini and R. Maartens, Mon. Not. Roy. Astron. Soc. **485**, 1339 (2019), 1812.01636.
- [36] B. Stözlner, A. Cuoco, J. Lesgourgues, and M. Bilicki, Phys. Rev. D **97**, 063506 (2018), 1710.03238.
- [37] S. Nakamura, A. De Felice, R. Kase, and S. Tsujikawa, Phys. Rev. D **99**, 063533 (2019), 1811.07541.
- [38] F. Giacomello, A. De Felice, and S. Ansoldi, JCAP **03**, 038 (2019), 1811.10885.